OPEN ACCESS



Tropical Cyclones on Tidally Locked Rocky Planets: Dependence on Rotation Period

Valeria Garcia^{1,2}, Cole M. Smith³, Daniel R. Chavas^{2,4}, and Thaddeus D. Komacek^{3,4} Department of Atmospheric Sciences, University of Washington, Seattle, WA 98195, USA

Department of Earth, Atmospheric, and Planetary Sciences, Purdue University, West Lafayette, IN 47907, USA

Department of Astronomy, University of Maryland, College Park, MD 20742, USA; tkomacek@umd.edu

Received 2023 October 27; revised 2024 February 19; accepted 2024 February 26; published 2024 April 1

Abstract

Tropical cyclones occur over the Earth's tropical oceans, with characteristic genesis regions and tracks tied to the warm ocean surface that provide energy to sustain these storms. The study of tropical cyclogenesis and evolution on Earth has led to the development of environmental favorability metrics that predict the strength of potential storms from the local background climate state. Simulations of the gamut of transiting terrestrial exoplanets orbiting late-type stars may offer a test of this Earth-based understanding of tropical cyclogenesis. Previous work has demonstrated that tropical cyclones are likely to form on tidally locked terrestrial exoplanets with intermediate rotation periods of $\sim 8-10$ days. In this study, we test these expectations using ExoCAM simulations with both a sufficient horizontal resolution of 0.47×0.63 required to permit tropical cyclogenesis along with a thermodynamically active slab ocean. We conduct simulations of tidally locked and ocean-covered Earth-sized planets orbiting late-type M dwarf stars with varying rotation periods from 4–16 days in order to cross the predicted maximum in tropical cyclogenesis. We track tropical cyclones that form in each simulation and assess their location of maximum wind, evolution, and maximum wind speeds. We compare the resulting tropical cyclone locations and strengths to predictions based on environmental favorability metrics, finding good agreement between Earth-based metrics and our simulated storms with a local maximum in both tropical cyclone frequency and intensity at a rotation period of 8 days. Our results suggest that environmental favorability metrics used for tropical cyclones on Earth may also be applicable to temperate tidally locked Earth-sized rocky exoplanets with abundant surface liquid water.

Unified Astronomy Thesaurus concepts: Atmospheric circulation (112); Exoplanet atmospheres (487); Planetary atmospheres (1244); Exoplanet atmospheric dynamics (2307)

Supporting material: animation

1. Introduction

Tropical cyclones are one of the most impactful weather phenomena on Earth, characterized by fast winds and heavy rainfall (Emanuel 2003). Tropical cyclones act as heat engines, powered by heat input from the warm ocean surface and dissipated via friction in the boundary layer between the atmosphere and surface (Emanuel 2003; Chavas 2017). On Earth, tropical cyclones may have large-scale impacts on the mean climate, most notably by drying surrounding regions (Schenkel & Hart 2015) and thereby enabling dry regions to more efficiently radiatively cool to space (Pierrehumbert 1995; Wing 2019). Tropical cyclones are also expected to form on tidally locked terrestrial exoplanets (Komacek et al. 2020; Yan & Yang 2020) and may have potential consequences for observable properties, especially the amplitude of water vapor features in transmission spectra (Yan & Yang 2020) as well as their time variability (May et al. 2021; Song & Yang 2021; Rotman et al. 2023).

Existing theories on the formation and evolution of tropical cyclones have identified a broad set of metrics for the environmental favorability required for tropical cyclogenesis to occur. These include the maximum potential intensity (Bister

Original content from this work may be used under the terms of the Creative Commons Attribution 4.0 licence. Any further distribution of this work must maintain attribution to the author(s) and the title of the work, journal citation and DOI.

& Emanuel 2002), genesis potential index (GPI; Emanuel 2010), ventilation index (Tang & Emanuel 2012), and ventilation-reduced potential intensity (Chavas 2017), along with more general quantities, including absolute vorticity (Hoogewind et al. 2020) and climate properties, including sea surface temperature (SST) and humidity (Camargo et al. 2014). These favorability metrics, especially the combination of absolute vorticity, maximum potential intensity, and ventilation index, can successfully match the observed regions of tropical cyclogenesis on Earth (Hoogewind et al. 2020). Recent work has calculated these favorability metrics from low-resolution general circulation model (GCM) simulations of tidally locked rocky exoplanets, finding that tropical cyclones should be unlikely to occur on slowly rotating exoplanets but peak in environmental favorability at intermediate rotation periods of \sim 8–10 days (Bin et al. 2018; Komacek et al. 2020).

Idealized experiments with a sufficient spatial resolution to permit tropical cyclones have investigated the dependence of cyclogenesis and intensity on key climate controls, including moisture availability and rotation rate (Reed & Chavas 2015; Merlis et al. 2016; Chavas & Reed 2019; Cronin & Chavas 2019). This approach can be extended to simulate the potential for tropical cyclogenesis in the atmospheres of terrestrial exoplanets. Notably, Yan & Yang (2020) conducted ≈50 km horizontal resolution GCMs of tidally locked terrestrial exoplanets with prescribed SST distributions. They found that, as expected from environmental favorability metrics, tropical cyclones may be common on terrestrial exoplanets with plentiful surface oceans. However, the prescribed day-

⁴ D.R.C. and T.D.K. contributed equally to this work.

night SST gradients in their simulations that produced tropical cyclones were smaller than might be expected from simulations with an interactive slab ocean. As a result, there is a need to further test our largely Earth-based understanding of tropical cyclogenesis using models with a thermodynamic ocean that cover a broader range of planetary parameters.

In this manuscript, we improve on Yan & Yang (2020) by conducting storm-resolving GCM simulations at an equivalent horizontal resolution but with a thermodynamically active slab ocean and thermodynamic sea ice scheme. We conduct GCMs of tidally locked planets with varying rotation periods in order to test the expectation from Earth-based environmental favorability metrics that tropical cyclone activity on tidally locked terrestrial exoplanets is most pronounced at intermediate rotation periods of \sim 8–10 Earth days. Specifically, we test the results of Komacek et al. (2020) by conducting otherwise equivalent GCMs but with sufficient horizontal resolution to permit tropical cyclogenesis. This work is organized as follows. We describe our GCM setup and tropical cyclone tracking algorithm in Section 2. In Section 3, we present results for how tropical cyclone location and intensity varies with rotation period and then compare our numerical simulations with environmental favorability metrics. We discuss the implications of our results as well as the limitations of our model setup in Section 4. Finally, we summarize our key points in Section 5.

2. Methods

2.1. GCM Simulations

In order to simulate the atmospheric circulation of tidally locked rocky exoplanets orbiting late-type M dwarf stars, we use the ExoCAM⁵ GCM (Wolf et al. 2022). ExoCAM has a broad heritage in this parameter regime (Kopparapu et al. 2017; Wolf 2017; Haqq-Misra et al. 2018; Komacek & Abbot 2019 Yang et al. 2019; Suissa et al. 2020; Wei et al. 2020; Wolf et al. 2020, 2022) and has participated in multiple broad 3D GCM intercomparison studies for the climates of potentially habitable rocky exoplanets orbiting M dwarf stars, including the TRAPPIST-1 Habitable Atmosphere Intercomparison project (Yang et al. 2019; Fauchez et al. 2022; Sergeev et al. 2022; Turbet et al. 2022). ExoCAM itself is a branch of the Community Atmosphere Model version 4, and it is coupled to ExoRT⁶, a flexible correlated-k radiative transfer routine that is applicable to exoplanet atmospheres near the inner edge of the habitable zone. ExoRT opacities are sourced both from HITRAN and the HELIOS-K opacity calculator (Grimm et al. 2021; Gordon et al. 2022).

In this work, we use ExoCAM and ExoRT to simulate the circulation of tidally locked rocky exoplanets solely as a function of the rotation period. Specifically, we conduct branch simulations from the ExoCAM GCMs presented in Komacek et al. (2020) with sidereal rotation periods of 4, 8, and 16 days. To do so, we interpolate the equilibrated GCM output from cases with a horizontal resolution of $4^{\circ} \times 5^{\circ}$ in Komacek et al. (2020) to a horizontal resolution of $0^{\circ}.47 \times 0^{\circ}.63$ in latitude and longitude, as in Komacek et al. (2019). This horizontal resolution has previously been demonstrated to permit tropical cyclones in GCM simulations of tidally locked terrestrial

planets with fixed SST (Yan & Yang 2020). All simulations use planetary parameters (besides rotation period/rate) that are identical to those of Earth, including a radius of 6.37122×10^6 m, surface gravity of 9.80616 m s⁻², and stellar constant of $1360 \,\mathrm{W\,m^{-2}}$. We set obliquity and eccentricity to zero, consistent with the assumption of tidal locking. Note that these idealized simulations do not consistently vary the incident stellar flux and rotation period (according to Kepler's third law, Kopparapu et al. 2017) in order to isolate the effect of the rotation period on tropical cyclogenesis. The atmospheric composition is set to have 1 bar of background N2, along with water vapor set by Clausius-Clapeyron, assuming an aquaplanet surface. All simulations use an incident stellar spectrum of a late-type M dwarf star with $T_{\rm eff} = 2600 \, \rm K$ (Allard et al. 2007). We further include a 50 m slab ocean⁸ and the CESM thermodynamic sea ice scheme (Bitz et al. 2001, 2012), while notably neglecting sea ice drift (Yang et al. 2020).

The simulations presented in this work use a dynamical time step of 30 minutes and a radiative time step of 1 hr. Each simulation has 40 vertical layers, spaced as in Komacek et al. (2020). We use 68 spectral intervals in the ExoRT correlated-k scheme (version src.cam.n68equiv), ranging from 0.238 μ m to ∞ . From the equilibrated initial state, we conduct simulations for 18 months. We only process the final 6 months of the simulation output in our analysis, while the first 12 months are discarded as an initial readjustment period. The analyses presented in this work focus on the 6 hr climatology used for studying both the structure of and tracking of tropical cyclones.

2.2. Cyclone Tracking

In order to track candidate tropical cyclones in our ExoCAM simulations, we process our GCM output with TempestExtremes (Ullrich et al. 2021). TempestExtremes is a generalized feature tracker that tracks tropical cyclones by defining features using closed contour criteria. Our tropical cyclone tracking process with TempestExtremes consists of two discrete steps. First, we search for potential locations of tropical cyclones in each of our 6 hr output time steps using the DetectNodes routine in TempestExtremes. Specifically, we search for closed contours around minima in surface pressure with a surface pressure decrement of at least 2 mbar from the environment. These minima must also have a geopotential contrast of $-58.8 \text{ m}^2 \text{ s}^{-2}$ between 300 and 500 mbar in order to ensure that they are warm-core storms (Zarzycki & Ullrich 2017). This second criterion is important to distinguish tropical cyclones from other low-pressure disturbances. We allow maximum closed contour widths of 6°, 12°, and 24° in cases with rotation periods of 4, 8, and 16 days, respectively. We increase the allowed closed contour width with a rotation period in order to account for the expected increase in storm size (Chavas & Reed 2019; Lu & Chavas 2022). We then stitch these detected low-pressure regions in time to form tropical cyclone trajectories with the StitchNodes routine in TempestExtremes. We choose a maximum range of 4° for tropical cyclone stitching over the 6 hr between output time steps, a minimum storm length of 24 hr, and a maximum gap between consecutive stitched points of 12 hr.

⁵ https://github.com/storyofthewolf/ExoCAM

⁶ https://github.com/storyofthewolf/ExoRT

Throughout this work, day refers to an Earth day.

 $[\]overline{^8}$ Komacek et al. (2020) previously demonstrated that using a shallow 1 m slab ocean depth does not affect predictions for tropical cyclogenesis, and thus, in this work, we only study cases with a thick slab ocean and resulting high surface heat capacity.

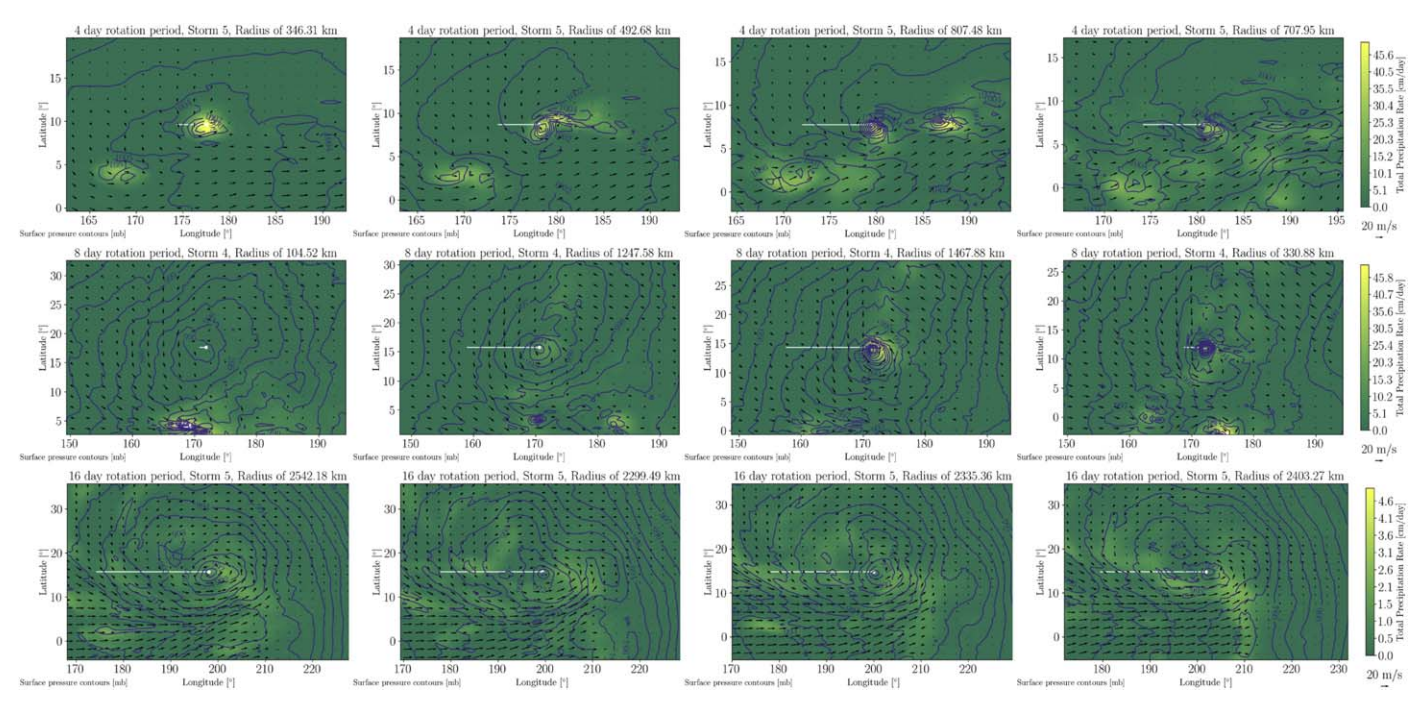


Figure 1. Snapshots of individual storms from cases with a rotation period of 4 days (top), 8 days (middle), and 16 days (bottom). The total precipitation rate is plotted in filled contours, the surface pressure (in millibars) is plotted in the blue contours, and near-surface wind speeds (in meters per second) are plotted in quivers. Snapshots are taken in 6 hr intervals, and each set of snapshots crosses the time of maximum intensification of the storm. The white bar demarcates the characteristic radius of the storm, which is further listed in the figure title. Note that the substellar longitude is 180°, and that the scaling of the longitude and latitude range and surface pressure changes between panels. Animations of the three storms are available in the online journal as a single file. Each animation displays the evolution of each of the three storms in order of increasing rotation period. These animations display the precipitation (filled contours), surface pressure (contour lines), and winds (quivers) in the region centered on the tracked storm. In the animation, snapshots from each 6 hr of model output are shown for the duration of the tracked storm. (An animation of this figure is available.)

3. Results

3.1. Tropical Cyclones with Varying Rotation Periods

Before studying the properties of the full sample of tracked storms from our simulations, we identified the five storms with the longest lifetime from each of the three simulations with varying rotation periods, labeling them by number in order of decreasing tracked point count (i.e., storm length). The horizontal structure, including surface pressure, surface winds, and precipitation, in one of the five storm case studies over the course of the 24 hr crossing the timing of maximum intensification for each simulation is shown in Figure 1.

As expected, the tracked storms are each cyclonic (with anticlockwise winds if in the northern hemisphere and clockwise winds in the southern hemisphere) and associated with a pressure decrease toward the center. The case study in the simulation with a rotation period of 8 days has the greatest pressure gradient from the center of the storm outward, along with the strongest winds as expected from the geostrophic balance. Note that some storms in the case studies with a rotation period of 8 days are accompanied by a cyclone in the southern hemisphere (not shown)—such dipolar cyclone, or *modon* (Cho et al. 2021) structure has been found in previous tidally locked planet GCMs.

The white bar in each panel of Figure 1 shows the characteristic radius of the storm, calculated as the radius where the azimuthal average of the winds decreases below 8 m s⁻¹. The characteristic radius increases with increasing rotation period in these specific case studies, as expected given the increase of the Rhines and inverse f-scales with rotation period (Chavas & Reed 2019; Lu & Chavas 2022). The

precipitation peaks around the pressure minimum in all cases. The storm intensity, measured by both the horizontal surface pressure minimum and wind speeds, is largest in the 8 day case. Additionally, the storms are more symmetric in the 8 day case than in the 4 and 16 day cases—in the 4 day case, the strong wind shear due to the super-rotating jet elongates the tropical cyclone, while in the 16 day case there is significant substructure in the storm at scales below the radius of the maximum wind. Notably, in the 4 day case, the wind quivers cross the center of the storm (rather than being in gradient wind balance), which demonstrates the influence of the background flow on the storm structure of this weaker cyclone.

Figure 2 shows azimuthally averaged vertical cross sections of cyclonic and radial wind speeds as well as relative humidity from the same storms shown in Figure 1. The vertical cross sections in Figure 2 are further shown from the same model output time as the horizontal profiles in Figure 1. All azimuthal averages are performed on isobars, and the cyclonic wind magnitude is specifically the azimuthal storm-centered average of the rotational (i.e., non-divergent) component in the Helmholtz decomposition (Hammond & Lewis 2021).

We find that the center of each storm is associated with a tower of high relative humidity extending to the top of the troposphere, as expected from the previous tropical cyclone-permitting simulations of Yan & Yang (2020). All storms have radial inflow near the surface and outflow at upper levels, as expected for tropical cyclones (Emanuel 2003). We also find a peak in the cyclonic wind speeds in the deep atmosphere adjacent to the center of the storm (i.e., an eyewall-like structure) in the case study with a rotation period of 16 days, as well as in other case studies with rotation periods of 4 and

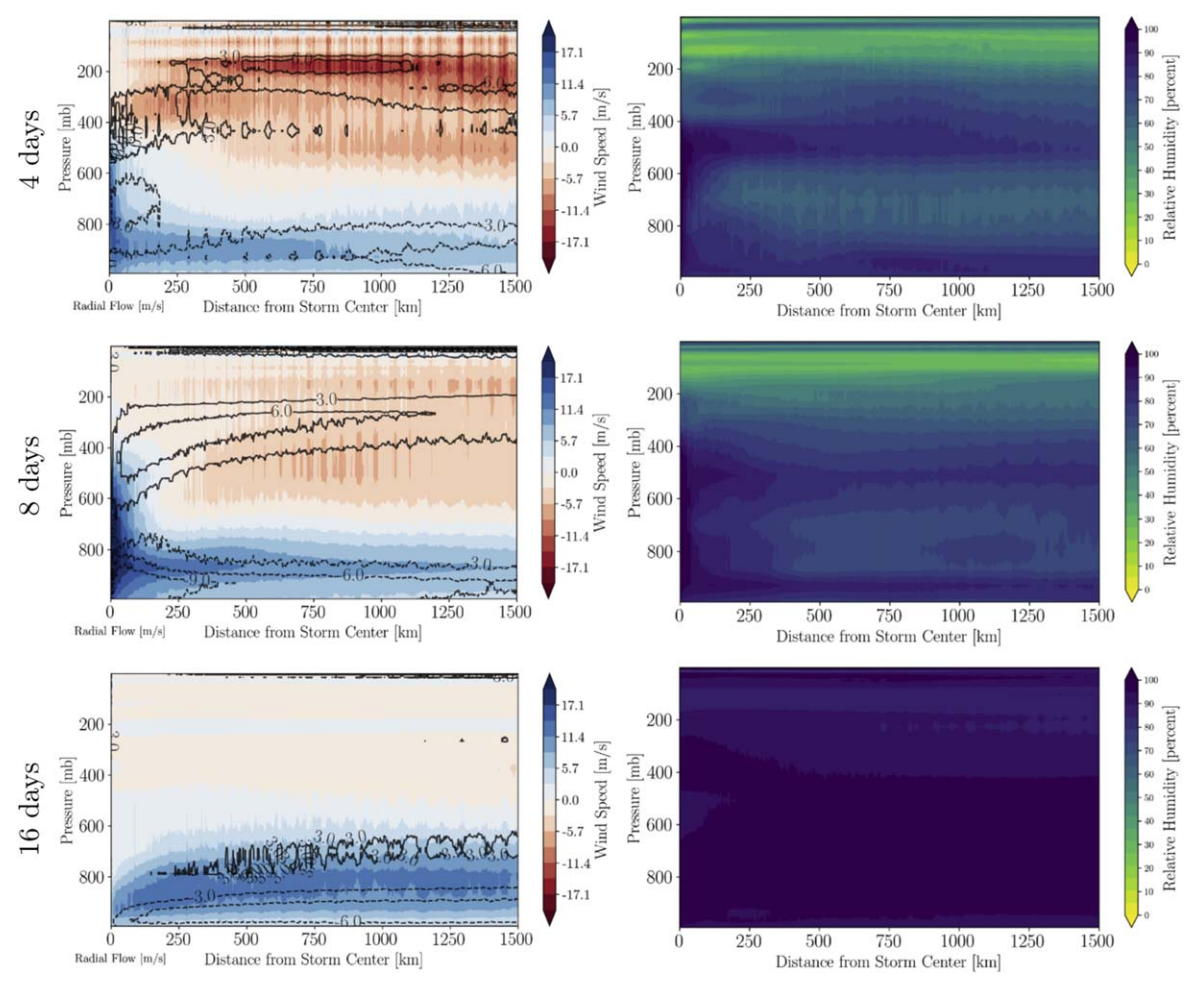


Figure 2. Storm-centered cross sections for the same storms in Figure 1 from cases with a rotation period of 4 days (top), 8 days (middle), and 16 days (bottom). Each vertical level is averaged azimuthally in circles around the tracked storm center. The left-hand panels display the azimuthally averaged cyclonic wind speed (in meters per second, with positive values representing cyclonic flow and negative values representing anticyclonic flow), and the right-hand panels display the azimuthally averaged relative humidity (in percent). The contour levels on the left-hand panel display radial wind speeds in meters per second, with inflow denoted by dashed contours and outflow by solid contours. The vertical axis is the atmospheric pressure (in millibars), and the horizontal axis is the distance from the tracked storm center (in kilometers). Each cross section shown is a snapshot at the time of maximum intensification in Figure 1.

8 days (not shown). In the fast-rotating cases with rotation periods of 4 and 8 days, we find that the presence of a superrotating jet at low pressures ventilates the top of the storm (note the band of small relative humidity at low pressures), limiting the height of the tropical cyclone. The 8 day case shows the best correspondence of horizontal and vertical structure to both expectations of tropical cyclones for Earth as well as the previous tidally locked exoplanet GCMs of Yan & Yang (2020). Overall, all of our case studies with varying rotation periods are tropical cyclone-like, consisting of a surface-based vortex that is strongest at small radii, with inflow at low levels and outflow at upper levels, a nearly saturated convecting column at the center, and (in some cases) an eye-like feature at the center.

To provide context, the location at which each tracked storm from the three simulations had its strongest horizontal wind is shown in Figure 3. We study the location of peak intensity rather than genesis because the location of peak intensity best corresponds to the distribution of where tropical cyclones can be supported by the environment. We also show tracking both, including and excluding the geopotential criterion in order to display the importance of including geopotential in tracking storms on tidally locked rocky planets. There are two classes of

tracked storms that are immediately distinguishable by comparing tracking with and without the geopotential criterion: tropical (warm-core) cyclones that form near the substellar point, and extratropical (cold-core) cyclones that form near the polar regions. We have visually verified that the extratropical cyclones are cold-core and associated with the Rossby gyres of the planetary-scale Matsuno–Gill pattern (Showman et al. 2013; Pierrehumbert & Hammond 2019).

As evident in Figure 3, all of the warm-core tropical cyclones in our three GCMs occur on the dayside, concentrated near the substellar point. The patterns of the tracked points differ between the cases with varying rotation periods, with the near-equatorial storms in the 4 day case concentrated closer to the equator, those in the 8 day case in a crescent that extends north and south from the substellar point, and those in the 16 day case concentrated in two regions northeast and southeast of the substellar point. As we discuss in Section 3.2, the locations of the maximum wind for the tropical cyclones are controlled by the background climate, and thus can be predicted from large-scale environmental favorability metrics. As we will show, the locations of storms move further from the equator in more slowly rotating cases due to the constraint of sufficient

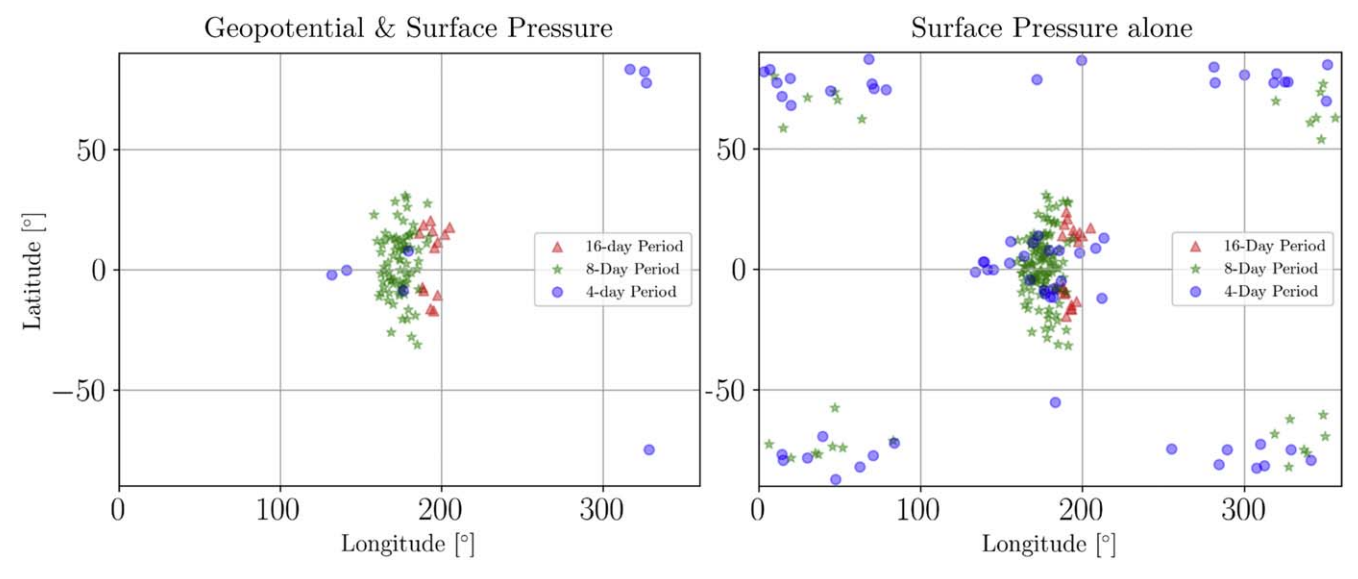


Figure 3. Location of where each tracked storm has its maximum total horizontal wind speed. The left-hand plot shows the results when including both surface pressure and geopotential criterion in the tracking, while the right-hand side shows the results from tracking that only considers surface pressure (and hence does not distinguish between warm- and cold-core storms). Cases with a period of 16 days are shown as red triangles, 8 day cases as green stars, and 4 day cases as blue circles. Storms near the polar regions in the surface pressure alone tracking are polar cyclones associated with the Rossby gyres of the planetary-scale Matsuno–Gill pattern, most commonly tracked in faster-rotating cases. All near-equatorial storms are found on the dayside, concentrated around the substellar point.

absolute vorticity, which is smaller near the equator due to a combination of slower rotation and weaker winds.

3.2. Comparison with Environmental Favorability Metrics

We compare our results to two separate environmental favorability metrics: the ventilation-reduced maximum potential intensity (a metric that incorporates the ventilation index to calculate a refined maximum potential intensity) and absolute vorticity. The ventilation-reduced maximum potential intensity provides the maximum achievable wind speed for a tropical cyclone in the presence of ventilation by dry air from its surroundings. The normalized ventilation-reduced maximum potential intensity can be written in a simpler form than Komacek et al. (2020) following some mathematical reduction:

$$u_{\rm p,VI} = \left(x + \frac{1}{3x}\right)u_{\rm p},\tag{1}$$

where

$$x = \frac{1}{\sqrt{3}} \left[\sqrt{\left(\left(\frac{\text{VI}}{\text{VI}_{\text{thresh}}} \right)^2 - 1 \right)} - \left(\frac{\text{VI}}{\text{VI}_{\text{thresh}}} \right) \right]^{\frac{1}{3}}, \tag{2}$$

and u_p is the maximum potential intensity (Bister & Emanuel 2002).

Equations (1) and (2) are derived from the equilibrium solution for normalized intensity in the presence of mid-level ventilation (Chavas 2017). Here VI is the ventilation index calculated as in Tang & Emanuel (2012). In Equation (2), VI_{thresh} is a threshold value of VI representing the maximum value of VI where $u_{\rm p,VI} > 0$, and no storm can be sustained. We set VI_{thresh} = 0.145, which was estimated based on Earth in Hoogewind et al. (2020) and used in Komacek et al. (2020). This solution can have both real and imaginary components; only the real component is physical and is used as the solution.

The top row of Figure 4 compares tropical cyclone locations using both surface pressure (labeled MSLP, 9) and surface pressure and geopotential together from Figure 3 to the 6 month mean of $u_{\rm p,VI}$ for each of the three cases. In this and all comparisons to environmental favorability metrics, we take the tropical cyclone location to be the location of peak intensity—i.e., where the storm has a maximum in its tracked 850 hPa horizontal wind speed. As mentioned in Section 3.1, this is because the location of maximum intensity will correspond to the point at which the storm is best supported by the environment.

We find that the simulated tropical cyclones cluster near the maxima of $u_{\rm p,VI}$, with especially good agreement in the case with a rotation period of 8 days. However, this metric alone does not explain the eastward shift of storms from the substellar point in the 4 and 16 day cases.

In order to determine the extent to which multiple metrics can explain tropical cyclone locations, we also compare our simulated tropical cyclone locations with the 6 month mean of the 850 mbar absolute vorticity η , which is simply the sum of the relative vorticity ξ and planetary vorticity f at that level:

$$\eta = \xi + f = \hat{k} \cdot (\nabla \times \mathbf{u}) + 2\Omega \sin(\phi). \tag{3}$$

In Equation (3), Ω is the rotation rate, ϕ is the latitude, \hat{k} is the unit vector in the vertical direction, and \mathbf{u} is the vector wind speed. The middle row of Figure 4 shows a comparison of the locations of simulated tropical cyclones with η . We find that the locations of storms in the 16 day case are well correlated with absolute vorticity maxima, and in the 4 day case, the maxima of absolute vorticity poleward of the substellar point better match with the tracked cyclone locations. However, there is a large clustering of storms near the substellar point in the 8 day case

Note that mean surface pressure and mean sea level pressure are equivalent in these aquaplanet simulations.

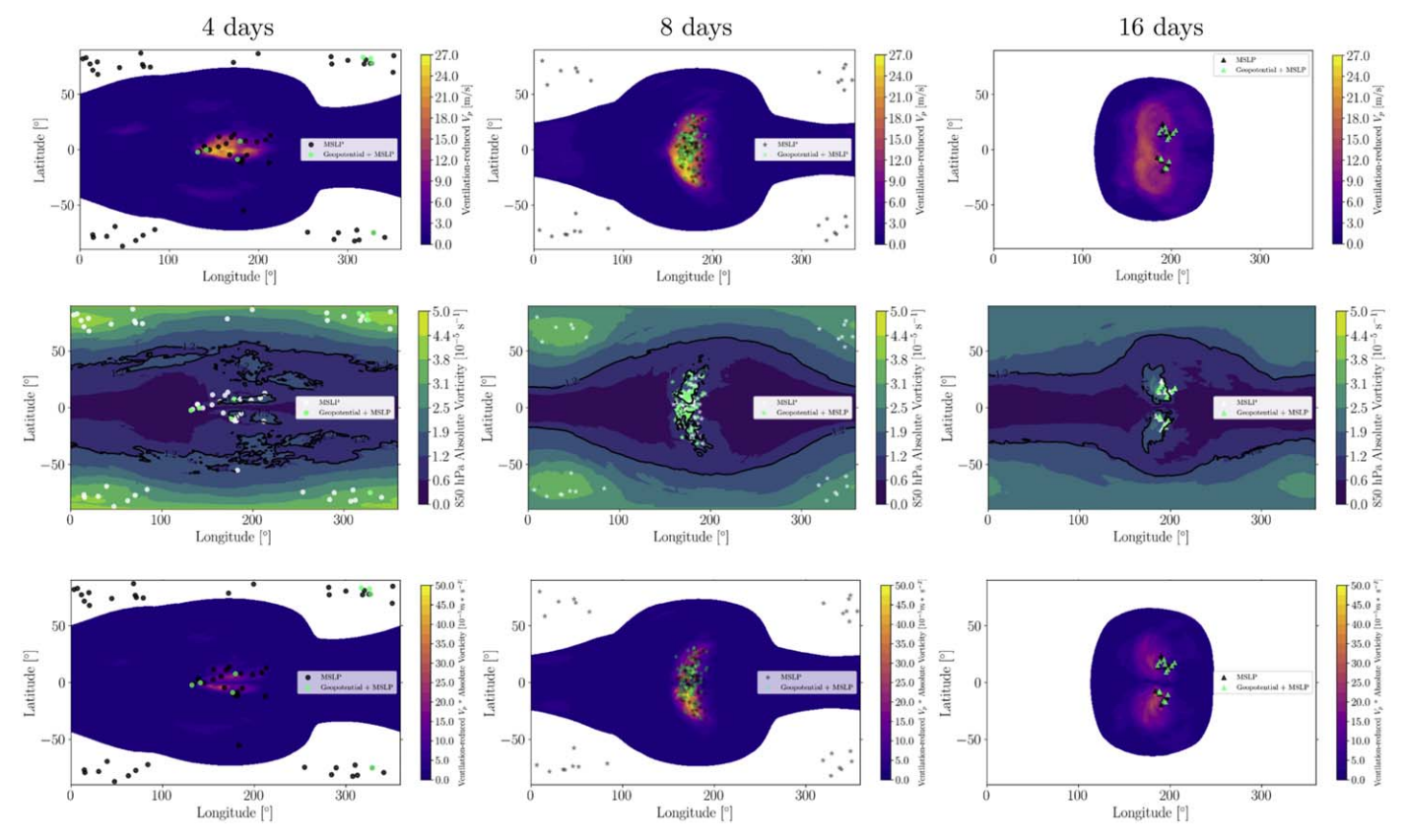


Figure 4. Comparison of environmental favorability metrics from the mean climate state to our tracked cyclone locations. Top row: 6 month mean ventilation-reduced maximum potential intensity (filled contours) for each case with varying rotation period, with locations of storms from Figure 3 overplotted, both from tracking with just surface pressure (MSLP) and both surface pressure and geopotential. Middle: same as the top row, but for absolute vorticity. Bottom: same as above, but for the product of ventilation-reduced maximum potential intensity and absolute vorticity. We find that warm-core tracked storm locations are generally found near the maxima in ventilation-reduced maximum potential intensity and the product of ventilation-reduced maximum potential intensity and absolute vorticity, with especially good agreement in the case with a rotation period of 8 days.

that is not well explained by absolute vorticity alone, as it peaks at higher latitudes.

We postulate that a simple product of absolute vorticity and ventilation-reduced maximum potential intensity, which is similar to existing GPIs, as shown in Komacek et al. (2020), may qualitatively describe the locations of simulated tropical cyclones. The bottom row of Figure 4 compares storm locations to the product $\eta \times u_{p,VI}$. We find that this combined metric provides the best overall match to the locations of tropical storms, especially in the 4 and 8 day cases. In the 16 day case, absolute vorticity alone is a better predictor of storm location than the combination of absolute vorticity and ventilation-reduced maximum potential intensity, as the surface area with sufficient absolute vorticity in this region is relatively small, and hence absolute vorticity is the primary bottleneck to genesis. Overall, we find that the case with a rotation period of 8 days has the best alignment between high ventilation-reduced potential intensity and high absolute vorticity, and hence the most coherent region of high favorability in the long-term mean of environmental properties that aligns remarkably well with actual tracked tropical cyclone activity.

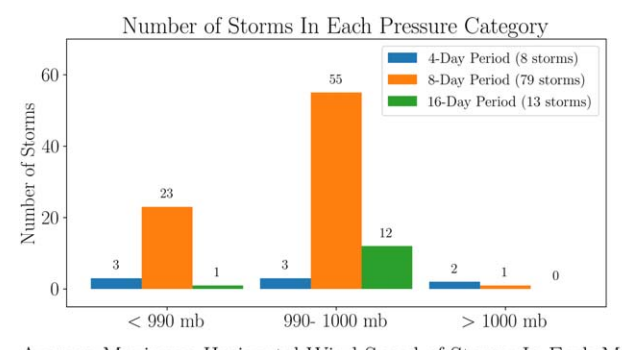
3.3. Tropical Cyclone Properties

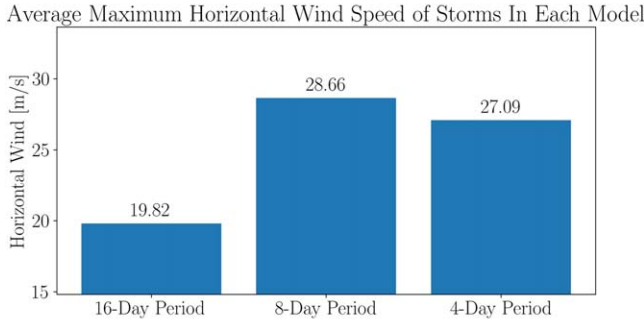
Finally, we summarize the intensity of storms with varying rotation periods with frequentist statistics. Figure 5 compares summary statistics for storms in each of our three simulations, focusing only on the tracking with both geopotential and

surface pressure constraints. 10 The top row counts the number of storms with sufficient minimum surface pressure (here equivalent to mean sea level pressure, MSLP) at any given point in their evolution to be classified as hurricanes (MSLP <990 mbar) according to the revised Saffir–Simpson Hurricane Wind Scale with modified MSLP (i.e., surface pressure) criteria of Klotzbach et al. (2020), along with storms of intermediate intensity (990 mbar < MSLP < 1000 mbar) and low intensity (MSLP >1000 mbar). We find that over the 6 month output time of the numerical experiments, the case with a rotation period of 8 days has the most tracked systems with surface pressures corresponding to hurricanes, as well as the most tracked storms with intermediate intensity. The 16 day case has the second-most storms with intermediate intensity, but zero hurricane-strength surface pressure decrements tracked over 6 months. Few warm-core storms form in the 4 day case, with only eight total storms tracked, but with a roughly equal distribution of intensities in our coarse pressure bins.

The middle row of Figure 5 shows a measure of the average peak intensity, measured as the average of the maximum wind speeds at 850 mbar within 4° of the tracked cyclone center in

¹⁰ Note that far more storms are tracked when considering surface pressure alone. In the 4 day case, 62 storms are tracked with just surface pressure, while only 8 are found with both surface pressure and geopotential. Similarly, for the 8 day case, 151 storms are tracked with just surface pressure and 79 with both surface pressure and geopotential, and in the 16 day case, 20 storms are tracked with just surface pressure constraints and 13 storms are tracked with both surface pressure and geopotential.





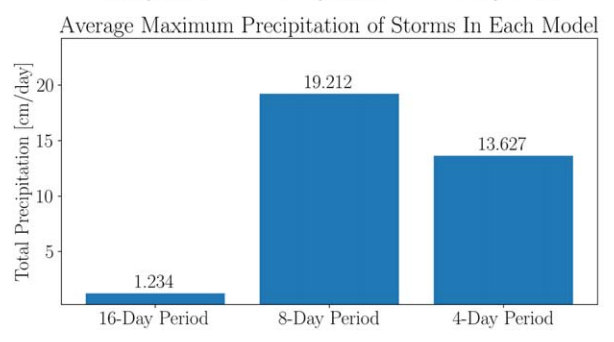


Figure 5. Summary histograms for the number distribution of minimum central tracked storm surface pressure with varying rotation periods (top), and the average of the maximum wind speeds from each storm (middle) and the average of the maximum precipitation from each storm (bottom). Results are shown for all tracked storms in our three cases with varying rotation periods. We find that the 8 day case has the most storms overall and the most storms with hurricane-level surface pressure, resulting in the highest average maximum horizontal wind speeds. The 4 day case has the highest average of the maximum precipitation in the tracked storms, potentially because this simulation has the warmest sea surface temperatures.

TempestExtremes. Additionally, the bottom row of Figure 5 shows the average peak precipitation within 4° of all storms for each case with varying rotation period. We find that the 8 day case has the greatest average storm wind speed, with the 16 day case having the weakest overall winds. The average maximum precipitation in the 8 day case is comparable to that of strong tropical cyclones on Earth, together with the wind speeds demonstrating that the bulk properties of tropical cyclones on exoplanets may not be dissimilar to those on Earth. Lastly, the 8 day case has the greatest average maximum precipitation, with the storms in the 16 day case conversely being associated with relatively little precipitation. The decrease in precipitation at longer rotation periods may be linked to the cooler SSTs in the slower-rotating cases due to the prevalence of dayside clouds (Yang et al. 2014, for results from GCM simulations with the same rotation period parameter sweep as conducted here, see Figure 9 of Komacek & Abbot (2019)), as previous fixed SST aquaplanet simulations have found that tropical cyclone precipitation correlates with SST (Stansfield & Reed 2021).

4. Discussion

4.1. Comparison to Previous Work

Our results generally agree well with the previous expectations of Bin et al. (2018) and Komacek et al. (2020) from applying environmental favorability metrics to low-resolution exoplanet GCMs. As expected from the calculation of GPI in the slowly rotating models with a rotation period of 28 days in Bin et al. (2018), we find that tropical cyclone intensity and number decrease sharply in our case with a rotation period of 16 days relative to faster-rotating cases. As expected from the work of Komacek et al. (2020), applying the ventilationreduced maximum potential intensity and absolute vorticity, we find that the number and intensity of tropical cyclones both peak in our intermediate rotation case with a rotation period of 8 days. The key difference in our methodology compared to Bin et al. (2018) and Komacek et al. (2020) is that the simulations presented here have sufficient horizontal model resolution to resolve and track tropical cyclones. One notable difference between our findings and previous work is that we find weak tropical cyclone-like features (in terms of structure) that form at a rotation period of 16 days—meanwhile, both Bin et al. (2018) and Komacek et al. (2020) predict that tropical cyclogenesis is not favorable at such slow rotation periods. Future work with convection-permitting models is needed to investigate the structure of our tropical cyclone features in the slowly rotating regime in order to determine the interplay between substellar convection and cyclogenesis.

We also find broad agreement with the fixed SST simulations presented in Yan & Yang (2020), as they find that cyclogenesis is prevalent in all models with intermediate or rapid rotation. The key difference between this work and that of Yan & Yang (2020) is that we find that tropical cyclones only occur on the dayside near the substellar point. Meanwhile, tropical cyclones in Yan & Yang (2020) can persist in nonirradiated regions near the terminator, likely because the nightside is hotter due to smaller prescribed day-to-night SST contrasts. Meanwhile, in our simulations, the nightside has a large enough ventilation index that the ventilation-reduced maximum potential intensity is near-zero or undefined, as the sea surface is cooler than the overlying atmosphere, and thus, the net heat flux is downward into the surface (Figure 4). This difference between our results and those in Yan & Yang (2020) may depend on the background climate state, and thus the assumed atmospheric abundance of carbon dioxide or other greenhouse gases is assumed to be zero in this work. In general, we expect that tropical cyclones are more likely to persist on the nightside in hotter and moister climates, given that for temperate terrestrial planets day-to-night temperature contrasts decrease with increasing irradiation (Haqq-Misra et al. 2018).

4.2. Utility of Earth-based Tropical Cyclogenesis Favorability Metrics

We find that Earth-based metrics of absolute vorticity, ventilation index, maximum potential intensity, and ventilation-reduced maximum potential intensity presented in Chavas (2017) and Hoogewind et al. (2020) accurately predict the locations of tropical cyclones on tropical cyclone-permitting models of tidally locked terrestrial exoplanets. Notably, the

ventilation-reduced maximum potential intensity (Chavas 2017; Komacek et al. 2020) is a novel metric that has been applied to exoplanet simulations before being verified for Earth. Additional work applying the ventilation-reduced maximum potential intensity back to Earth itself finds good agreement with observed tropical cyclone genesis locations (D. R. Chavas et al. 2024, in preparation). Continued exoplanet-specific and idealized simulations of tropical cyclones may provide further insight into the properties that govern tropical cyclone behavior on Earth.

4.3. Limitations and Future Work

Though we improve on previous work by conducting tropical cyclone-permitting simulations of tidally locked exoplanets with thermodynamic ocean and sea ice schemes, our model setup is still idealized in many respects. Notably, we do not include a dynamic ocean with motions forced by wind stress from the overlying atmosphere, which has been shown to result in a characteristic eastward offset in the SST maximum (known as a *lobster* planet, Hu & Yang 2014). We also assume an aquaplanet and thus do not include any continents in our simulations, which have been shown to potentially have a large effect on moisture availability and surface enthalpy fluxes (Lewis et al. 2018; Salazar et al. 2020; Macdonald et al. 2022). We anticipate that including a dynamic ocean and/or continents may shift the region of tropical cyclone favorability toward the regions near the equator with the warmest SSTs. In the case of a large substellar continent, it is possible that the low heat capacity (sensible plus latent), along with the limited availability of moisture and lack of oceanic latent heat fluxes of the surface, may prevent tropical cyclogenesis. Future work is needed to simulate the impact of dynamic oceans and continent distribution on the prevalence of tropical cyclones on tidally locked terrestrial planets. In addition, further simulations are needed to assess the potential for tropical cyclogenesis on specific nearby temperate rocky exoplanets, including Proxima Centuari b, TRAPPIST-1e, and LP 890-9 c.

Our global GCMs are near the low end of the level of resolution required to resolve the basic structure of tropical cyclones, and in global models, the resolution may impact the frequency and intensity of tropical cyclones (Vecchi et al. 2019). In addition to being coarse in horizontal resolution, our simulations use the hydrostatic primitive equations and thus would not be convection-permitting even at higher resolutions. Future work is needed to study the potential for tropical cyclogenesis in higher-resolution models of tidally locked terrestrial planets, including local convection-resolving large eddy simulations (Lefèvre et al. 2021), global convectionresolving simulations (Yang et al. 2023), or global simulations with nested grids (Sergeev et al. 2020). Such work would facilitate a comparison between coarse global tropical cyclonepermitting simulations and tropical cyclone-resolving and convection-permitting simulations in order to determine the extent to which the methods used in this work are broadly applicable to study tropical cyclogenesis on tidally locked terrestrial exoplanets.

5. Conclusions

In this work, we conducted GCM simulations of tidally locked terrestrial exoplanets with a thermodynamically active slab ocean and sufficient spatial resolution to permit tropical

cyclogenesis. We conducted simulations with varying rotation periods of 4–16 days, and found that tropical cyclones occur in each simulation. We further find that the number and strength of tropical cyclones in each simulation agree with that predicted from Earth-based environmental favorability metrics. Our key conclusions are as follows:

- 1. Tropical cyclones occur in our ExoCAM GCM simulations of tidally locked terrestrial exoplanets orbiting late-type M dwarf stars that have a sufficient horizontal resolution to permit tropical cyclogenesis. Notably, these GCM simulations include a slab ocean, while previous work by Yan & Yang (2020) used a prescribed SST distribution. Thus, we extend the finding of Yan & Yang (2020) that tropical cyclones occur in fixed SST GCMs of tidally locked terrestrial exoplanets to simulations with thermodynamically consistent SSTs.
- 2. All tropical cyclones in our GCM experiments occur on the dayside of the planet, near the substellar point. The locations of the simulated tropical cyclones broadly match with environmental favorability metrics based on Earth and resulting predictions from the low-resolution simulations of Komacek et al. (2020), especially the combination of the ventilation-reduced maximum potential intensity and the absolute vorticity. Notably, we do not find warm-core tropical cyclones near the poles and on the nightside, but they did form in the fixed SST simulations of Yan & Yang (2020). The lack of tropical cyclones on the cooler poles and nightside is in agreement with expectations based on the ventilation index, which is small or undefined in these regions due to a thermal inversion in the boundary layer.
- 3. The dependence of the number and strength of tropical cyclones on the rotation period matches well with the expectations from the low-resolution GCMs studied in Bin et al. (2018) and Komacek et al. (2020). We find a peak in both the occurrence of tropical cyclones and their mean wind speeds in the case with an intermediate rotation period of 8 days. This local maximum in tropical cyclone intensity and number agrees with expectations from the coherent alignment of regions of high values of ventilation-reduced maximum potential intensity and absolute vorticity. The case with a rotation period of 4 days has an intermediate number of storms compared to the two slower-rotating cases, and storms in this fastrotating case are associated with the highest average maximum precipitation. We further find no tropical cyclones with hurricane-force winds in the slow-rotating case with a rotation period of 16 days, as expected from the combination of a small absolute vorticity and weak maximum potential intensity.

Acknowledgments

We thank Eric Wolf for making ExoCAM freely available to the community and continuing its development. We thank the anonymous referee for the insightful comments and suggestions, which greatly improved the manuscript. We thank Tobi Hammond and Julianna Heptinstall for their helpful feedback on this work. We acknowledge generous support from the Heising-Simons Foundation as part of the 51 Pegasi b Fellowship Enhancements. C.M.S. and T.D.K. are grateful to have received support from the 2023 Burgers Program Summer

Research Scholarships. We acknowledge high-performance computing support from Cheyenne (Computational and Information Systems Laboratory 2019) provided by NCAR's Computational and Information Systems Laboratory, sponsored by the National Science Foundation under NSF AGS grant No. 2209052. We acknowledge the University of Maryland supercomputing resources http://hpcc.umd.edu) made available for conducting the research reported in this paper.

ORCID iDs

Daniel R. Chavas https://orcid.org/0000-0001-9172-8328 Thaddeus D. Komacek https://orcid.org/0000-0002-9258-5311

References

```
Allard, F., Allard, N., Homeier, D., et al. 2007, A&A, 474, L21
Bin, J., Tian, F., Lin, Y., & Wang, Y. 2018, Icar, 299, 364
Bister, M., & Emanuel, K. 2002, JGRD, 107, 4801
Bitz, C., Holland, M., Eby, M., & Weaver, A. 2001, JGR, 106, 2441
Bitz, C., Shell, K., Gent, P., et al. 2012, JCli, 25, 3053
Camargo, S. J., Tippett, M. K., Sobel, A. H., Vecchi, G. A., & Zhao, M. 2014,
   JCli, 27, 9171
Chavas, D. 2017, JAtS, 74, 2989
Chavas, D., & Reed, K. 2019, JAtS, 76, 2257
Cho, J., Skinner, J., & Thrastarson, H. 2021, ApJL, 913, L32
Computational and Information Systems Laboratory 2019, Cheyenne: HPE/
   SGI ICE XA System (University Community Computing) (Boulder, CO:
   National Center for Atmospheric Research),
Cronin, T., & Chavas, D. 2019, JAtS, 76, 2193
Emanuel, K. 2003, AREPS, 31, 75
Emanuel, K. 2010, JAMES, 2, 1
Fauchez, T. J., Villanueva, G. L., Sergeev, D. E., et al. 2022, PSJ, 3, 213
Gordon, I. E., Rothman, L. S., Hargreaves, R. J., et al. 2022, JQSRT, 277,
Grimm, S. L., Malik, M., Kitzmann, D., et al. 2021, ApJS, 253, 30
Hammond, M., & Lewis, N. 2021, PNAS, 118, 2022705118
Haqq-Misra, J., Wolf, E., Joshi, M., Zhang, X., & Kopparapu, R. 2018, ApJ,
   852, 67
Hoogewind, K., Chavas, D., Schenkel, B., & O'Neill, M. 2020, JCli, 33, 1725
Hu, Y., & Yang, J. 2014, PNAS, 111, 629
Klotzbach, P., Bell, M., Bowen, S., et al. 2020, BAMS, 101, E830
```

```
Komacek, T., & Abbot, D. 2019, ApJ, 871, 245
Komacek, T., Chavas, D., & Abbot, D. 2020, ApJ, 898, 115
Komacek, T., Jansen, M., Wolf, E., & Abbot, D. 2019, ApJ, 883, 46
Kopparapu, R., Wolf, E., Arney, G., et al. 2017, ApJ, 845, 5
Lefèvre, M., Turbet, M., & Pierrehumbert, R. 2021, ApJ, 913, 101
Lewis, N., Lambert, F., Boutle, I., et al. 2018, ApJ, 854, 171
Lu, K.-Y., & Chavas, D. 2022, JAtS, 79, 2109
Macdonald, E., Paradise, A., Menou, K., & Lee, C. 2022, MNRAS, 513,
May, E., Taylor, J., Komacek, T., Line, M., & Parmentier, V. 2021, ApJL,
   911, L30
Merlis, T. M., Zhou, W., Held, I. M., & Zhao, M. 2016, GeoRL, 43, 2859
Pierrehumbert, R. T. 1995, JAtS, 52, 1784
Pierrehumbert, R. T., & Hammond, M. 2019, AnRFM, 51, 275
Reed, K. A., & Chavas, D. R. 2015, JAMES, 7, 1938
Rotman, Y., Komacek, T. D., Villanueva, G. L., Fauchez, T. J., & May, E. M.
   2023, ApJL, 942, L4
Salazar, A., Olson, S., Komacek, T., Stephens, H., & Abbot, D. 2020, ApJL,
   896, L16
Schenkel, B. A., & Hart, R. E. 2015, JCli, 28, 7529
Sergeev, D., Lambert, F., Mayne, N., et al. 2020, ApJ, 894, 84
Sergeev, D. E., Fauchez, T. J., Turbet, M., et al. 2022, PSJ, 3, 212
Showman, A., Wordsworth, R., Merlis, T., & Kaspi, Y. 2013, in Comparative
   Climatology of Terrestrial Planets, ed. S. Mackwell, A. Simon-Miller,
  J. Harder, & M. Bullock (Tucson, AZ: Univ. Arizona Press)
Song, X., & Yang, J. 2021, FrASS, 8, 134
Stansfield, A. M., & Reed, K. A. 2021, JGRD, 126, e2021JD035197
Suissa, G., Mandell, A., Wolf, E., et al. 2020, ApJ, 891, 58
Tang, B., & Emanuel, K. 2012, BAMS, 93, 1901
Turbet, M., Fauchez, T. J., Sergeev, D. E., et al. 2022, PSJ, 3, 211
Ullrich, P., Zarzycki, C., McClenny, E., et al. 2021, GMD, 14, 5023
Vecchi, G. A., Delworth, T. L., Murakami, H., et al. 2019, ClDy, 53, 5999
Wei, M., Zhang, Y., & Yang, J. 2020, ApJ, 898, 156
Wing, A. A. 2019, CCCR, 5, 1
Wolf, E. 2017, ApJL, 839, L1
Wolf, E., Haqq-Misra, J., Kopparapu, R., et al. 2020, JGRE, 125,
   e2020JE006576
Wolf, E., Kopparapu, R., Haqq-Misra, J., & Fauchez, T. 2022, PSJ, 3, 7
Yan, M., & Yang, J. 2020, A&A, 643, A37
Yang, H., Komacek, T., & Abbot, D. 2019, ApJL, 876, L27
Yang, J., Boue, G., Fabrycky, D., & Abbot, D. 2014, ApJL, 787, L2
Yang, J., Ji, W., & Zeng, Y. 2020, NatAs, 4, 58
Yang, J., Leconte, J., Wolf, E. T., et al. 2019, ApJ, 875, 46
Yang, J., Zhang, Y., Fu, Z., et al. 2023, NatAs, 7, 1070
Zarzycki, C., & Ullrich, P. 2017, GeoRL, 44, 1141
```